International Journal of Architectural Heritage

Conservation, Analysis, and Restoration

ISSN: 1558-3058 (Print) 1558-3066 (Online) Journal homepage: http://www.tandfonline.com/loi/uarc20

Discrete Element Analysis of the Minimum Thickness of Oval Masonry Domes

József Simon & Katalin Bagi

INTERNATIONAL JOURNAL OF ARCHITECTURAL HERITAGE
2016, VOL. 10, NO. 4, 457–475
http://dx.doi.org/10.1080/15583058.2014.996921

Taylor & Francis
Taylor & Francis Group

Discrete Element Analysis of the Minimum Thickness of Oval Masonry Domes

József Simon[a] and Katalin Bagi[b]

[a]Department of Structural Engineering, Budapest University of Technology and Economics, Budapest, Hungary; [b]Department of Structural Mechanics, Budapest University of Technology and Economics, Budapest, Hungary

ABSTRACT
This study focuses on domes the ground plan of which, instead of the more common circular shape, is an oval, and aims at finding the minimally necessary uniform wall thickness for domes of different geometries loaded by their selfweight. The discrete element code 3DEC was applied because of its capability of simulating the collapse mechanisms of masonry structures. Results on the minimal wall thickness, corresponding masonry volume and failure mechanisms for different dome geometries are presented. Three ranges of the friction coefficient were found. For very low frictional resistance collapse happens with pure frictional sliding, for any arbitrarily large wall thickness. In the range of relatively high (i.e., realistic) friction coefficients the structure collapses without any sliding if the wall is not sufficiently thick, and in the observed range of the friction coefficient the necessary wall thickness is nearly insensitive to its value (collapse initiates with hinging cracks only). Between the two domains an intermediate behavior was found: combined cracking and sliding collapse modes occur for insufficient wall thickness, and the minimal thickness strongly depends on the friction coefficient. The critical and transitional friction coefficients separating the failure modes were determined for different eccentricities of the groundplan.

ARTICLE HISTORY
Received 28 August 2014
Accepted 07 December 2014

KEYWORDS
3DEC; brick; distinct element; stone; structural stability

1. Introduction

While mathematicians use the term "oval" in a very general sense (e.g., Descartes or Cassini ovals, Lamé ellipsoids; see for instance in Lawrence, 1972), in architecture an oval is usually understood as a closed, convex, smooth curve having two axes of symmetry. A thorough overview was given by Huerta (2007) on the history of the application of oval shapes in different structural roles in architecture from the first civilizations until the Baroque. In this article, the role of ovals will be to provide the ground plan of a dome.

Although most of the existing domes of our architectural heritage have a circular plan, oval plans are more common than they are usually thought to be. As emphasized by Huerta (2007), already in the Middle Ages hundreds of Romanesque churches were built with oval plan (Chappuis, 1976); then in the Renaissance and in the Baroque the idea became even more popular and quickly spread all over Europe. In spite of this, their mechanical behavior (particularly the similarities to and differences from spherical domes) is hardly analyzed and hence poorly understood.

Masonry domes—similarly to masonry arches and vaults—are constructions of separate voussoirs supporting each other basically by compression and friction. Even if some kind of mortar is applied in the joints, its tensile strength is negligibly small compared to the compressive strength of the bricks or stones, particularly in the case of historical buildings with centuries or millennia old mortar in the joints. The compressive strength of the voussoirs can practically be considered infinite. (Of medium sandstone, a 2 km high column can be built without crushing at its base due to its own weight. For granite this height is 10 km according to Heyman, 2001, and even for different bricks this height is hundreds of meters, while the height of existing masonry domes and vaults does not exceed a few dozens of meters.) The frictional resistance is usually rather high even for dry joints (the angle of friction is at least approximately 30°–50°); indeed, sliding failure under static loads is not characteristic for domes and vaults. Hence, the basic question of the safety analysis of such a dome is whether the structure with its given geometry is able to equilibrate its self weight and perhaps certain live loads without cracking collapse. This is a question of stability rather than a problem of strength: "Equilibrium is achieved by geometry" (Huerta, 2001).

Keeping these specific features in mind, Heyman (1967, 1995) derived the minimal thickness of spherical

CONTACT Katalin Bagi kbagi@mail.bme.hu Department of Structural Mechanics, Budapest University of Technology and Economics, H-1111 Budapest, Műegyetem rkp. 3. K.mf. 63, Hungary.
Color versions of one or more of the figures in this article can be found online at www.tandfonline.com/uarc.

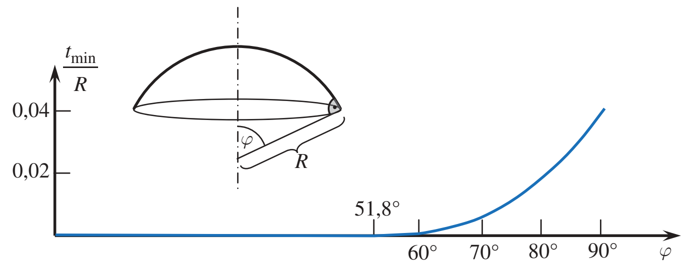

Figure 1. Minimal thickness for spherical domes, after Heyman (1967).

domes (see Figure 1). The problem he solved can be formulated as follows.

- Consider a spherical dome with a vertical axis of symmetry, characterized by the angle φ shown in Figure 1, with uniform thickness t.
- The material obeys the following basic assumptions (e.g., Boothby, 2001):
  - The blocks are perfectly rigid.
  - The blocks have infinite compressive strength.
  - The joints have infinite frictional resistance.
  - The joints have zero tensile strength.
- No translations are allowed at the supports at the base of the dome.
- The aim is to find the smallest thickness, $t_{\min}$, for which the dome is still in equilibrium under its own weight.

Heyman solved the problem using the Static Method of plastic limit analysis (e.g., Heyman, 1995; Huerta, 2001), and for $\varphi = 90°$ friction angle he found that this minimal thickness is 0.042 times the radius of the spherical surface.

Heyman made no distinction between the radii of the intrados, extrados, and middle surface. Indeed, $t_{\min}$ is so small in comparison with the radius of the dome that for an engineer the difference may seem to be negligible. Since in his derivations of the minimum thickness for arches (e.g., Heyman, 1969) the radius was defined to be measured to the center line of the arch, the same can be assumed for his studies on domes, which is in agreement with the usual convention in membrane theory where the middle surface gives the basis of the calculations. Consequently, the above value 0.042 is understood as the ratio of the minimal wall thickness vs. the radius of the middle surface.

An important improvement of Heyman's result was provided by Lau (2006), who, by combining membrane theory with the Static Method and hence taking into consideration hoop forces as well, received a slightly different value, 0.041 times the radius in the case of a hemispheral dome.

The safety of an analyzed dome can then be estimated by using the "factor of geometrical safety", invented also by Heyman (1969), originally introduced for arches. This factor compares the actual thickness of the structure to the minimal thickness which can still carry its own weight. (When live loads have to be considered, the minimal thickness belonging to the worst position of the loads has to be found. However, the dominant load on a dome is usually its self weight.) Although the assumption of uniform thickness is not always realistic for existing structures, even in these cases the geometrical factor of safety provides an intuitive measure for the engineer of how safe an actual structure is. The dome of the Roman Pantheon has, for instance, a wall thickness varying from top to bottom between about 5.5–30% of the radius; these values are far above the necessary minimal thickness. The thickness of the oval dome of the sanctuary of Vicoforte, as another example, is significantly smaller (and does not vary this much). Comparing to the equivalent groundplan radius, i.e., to the radius of the circle having the same area as the groundplan of the dome, the thickness is approximately 7–12% (Aoki et al., 2003). The knowledge of the necessary minimum thickness helps the engineer in appraising the safety of the structure. So the basic aim of the present study was to extend Heyman's problem to domes with oval plans (see the applied restrictions on the dome geometry in Section 2.1), and to find the minimal thickness for those cases.

To provide a possible method for the analysis of oval domes, Huerta (2010) called the attention on the transformation theorem of Rankine: "If a structure of a given figure have stability of position under a system of forces represented by a given system of lines, then will any structure, whose figure is a parallel projection of that of the first structure, have stability of position under a system of forces represented by the corresponding projection of the first system of lines." In general, this theorem could be useful for predicting the stability of an oval dome constructed by an affine transformation from a spherical dome. Obviously, it is not reliably applicable to the problem of the present study for several reasons:

- the plan composed of circular arcs is not an affine transformation of a single circular plan;
- the "stability of friction" of the transformed structures is not ensured by the theorem, i.e., the forces on the joints between individual blocks may or may not be inside the friction cone independently of the stability of friction of the original spherical dome; and
- the uniform thickness of a spherical dome would be distorted by an affine transformation.

Different recent numerical methods can be found in the literature to solve the problem of minimal wall thickness. The most important approaches are shortly overviewed below.

→ 3D Thrust Network Analysis (TNA, see Block and Ochsendorf 2007) and its extension in Block and Lachauer (2014) are based on the Static Theorem of Heyman's classical theory of masonry structures. The method applies three-dimensional graphic statics to find a thrust surface. The power of this method is convincingly demonstrated by Block et al. (2010) with the help of 3D-printed structural models. (Its disadvantage is that the possibility of sliding is not excluded with sufficient safety.)

→ With an improvement over membrane theory by allowing hoop and meridional forces to deviate from the middle surface, an iterative computation is used by Zessin et al. (2010) to analyze cracked masonry domes.

→ D'Ayala and Casapulla (2001) derived a proof that under a symmetry requirement for the loads, sliding mechanisms may be included in the limit state analysis of masonry domes without loss of uniqueness. A lower-bound computer method is proposed by the authors who apply their method for Heyman's problem extended to the effect of different friction coefficients in the joints. An interesting result is that if the friction coefficient is between 0.12 – 0.7, the minimal thickness can be smaller than derived by Heyman. Based on the success of the method, D'Ayala and Tomasoni (2011) presented a computational procedure and convincingly apply it for pavilion vaults, also giving a comparison to FEM results. The method has the potential to analyze problems with general loads and constraints, recognize sliding as well as hinging collapse mechanisms, and incorporate the three-dimensional effects for a wide range of vault types.

→ Another alternative tool which is also capable of modeling 3D effects and frictional sliding is the Discrete Element Method. This numerical technique was first introduced for the simulation of fractured rocks by Cundall (1971), and has been applied in the engineering practice approximately from the 1990s, when computer hardware became powerful enough to simulate realistic problems on average PCs. A discrete element model considers the structure to be a collection of separate blocks, "discrete elements," each of which is able to move and—in most software—to deform independently of each other. The blocks may come into contact with each other, where distributed forces can be transmitted from one block to another, causing stresses and deformations in the blocks. According to the criteria formulated by Cundall and Hart (1992), a numerical technique is a discrete element model if (1) the elements are able for finite (i.e., large) translations and rotations; and (2) complete detachment as well as formulation of new contacts are allowed and automatically followed.

The second criterion means two important differences from FEM: there are no continuity conditions at the common points of the contacting elements, and the elements are continuously checked throughout the calculations whether they get into contact with each other.

The large displacements are usually followed with the help of some kind of a time-stepping scheme: most DEM codes determine the characteristic motions of the analyzed system along a series of small but finite time intervals, applying Newton's laws of motion. Using DEM, a simulated structure may split into pieces (e.g., a vault may fall into masonry voussoirs) which may even bounce into each other on the ground forming a heap balanced under its own weight. There are innumerable different versions of discrete element techniques—the elements may be rigid or deformable, spherical, polyhedral, or irregular, the time integration may be explicit or implicit, or may be replaced by a quasi-static method, etc. A helpful introduction is given by O'Sullivan (2011) on the most important techniques. (A particular value of this book is that the issue of numerical stability, which is particularly important in the stability analysis of masonry vaults and domes, is discussed in detail.) An excellent overview is given by Lemos (2007) on the different mathematical and practical approaches to simulate masonry structures with the help of DEM, including practical engineering applications as well. The method has been successfully applied in practice-inspired investigations like Alexakis and Makris (2013) or Isfeld and Shrive (2015). In relation to the subject of the present paper, the study of Rizzi et al. (2014) has to be referred to in which the authors successfully apply the method for the analysis of the Couplet-Heyman problem, taking into account the effect of the frictional resistance between voussoirs.

Despite the few doubts regarding its usage (e.g., Huerta 2008), the capability to simulate block separation and contact sliding makes a suitably chosen and carefully calibrated DEM model a powerful tool for the collapse analysis of masonry structures. Because of its ability to follow frictional sliding, failure processes and collapse histories in detail, DEM has been the basic tool of the investigations of the authors related to different masonry mechanics problems, including the subject of the present paper. Details of the applied numerical technique are introduced in Section 3. It has to be emphasized that the model verification and within this the careful calibration of model parameters is a crucial issue in DEM modeling; this is why Section 3 puts a particularly strong emphasize on the question.

Before turning to the details of the analysis, two important aspects regarding Heyman's problem have to be underlined. First, Heyman assumed fixed supports under the domes. In reality, the supports always move: deformations of the underlying walls, soil sinking, etc. are inevitable. As a result, the masonry dome—whose voussoirs have only rather low if not negligible deformability—adjusts itself to the new position of the supports by cracking leading to the rearrangement of the internal force system. Consequently, the limit thickness for a dome with deforming supports will differ from Heyman's solution for the same dome. The analysis of the effect of support flexibility is out of the scope of the present study; it is left for further research and the present study is restricted to the original problem with fixed supports. However, sliding between the dome blocks and the fixed supports is allowed according to the Coulomb model.

Second, in reality the voussoirs are never infinitely rigid, so if the dome is built with the help of centering, a slight deformation always occurs at de-centering, hence modifying the shape of the dome. This effect may also lead to deviations of the minimal thickness from that of Heyman. In the DEM investigations the deformability of the voussoirs was not taken into account: the blocks were perfectly rigid, and the numerical control parameters of the model were carefully verified to match the result of Heyman's value for orange-sliced hemispherical domes. This calibrated model was then used for the simulation of oval domes.

This article is organized as follows. The analyzed geometries are specified in Section 2. Section 3 describes the most important characteristics of the utilized discrete element code (3DEC), and introduces the calibration tests which were done to ensure the reliability of the results; these numerical experiences may be helpful for researchers simulating other types of masonry vaults and domes with the help of DEM. The simulation results on oval domes are presented and discussed in Section 4. Finally, the most important conclusions are summarized in Section 5.

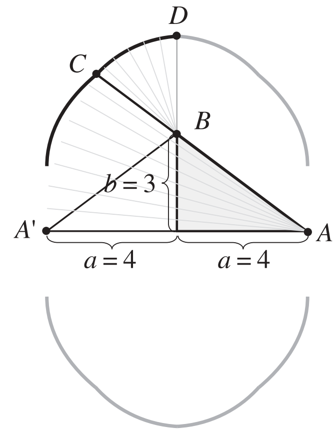

Figure 2. The Egyptian oval.

2. Preparation of the model geometry

2.1. Definition of the ground plan

The aim of this section is to introduce the mathematical definition of the ovals serving as plans for the domes to be analyzed. The most important versions, i.e., the Egyptian oval and its generalized versions which were applied in the present study, are described here in detail; other ovals being out of the scope of the present article are only shortly mentioned.

The Egyptian oval is based on a right-angled triangle whose sides are 3, 4, and 5 units. The quarter of the oval can be drawn, as shown in Figure 2, with the help of two pegs fixed at points A and B, and with an 8-unit long string whose beginning point is attached to the peg at point A.

Starting from point A', draw a circular arc (with 8-unit radius) by moving the endpoint of the string upwards, until the string is stopped by the peg at point B. The end of the string is now at point C. Continue moving this endpoint of the string further upwards; because of the peg at B, the radius of this new arc (from C to D) is only 3 units. The two arcs drawn this way will have a common tangent at point C, so the curve is smooth The rest of the oval can be prepared in the same way.

Right-angled triangles with other side ratios can also be applied as the basis of an oval: different generalized Egyptian ovals can be received this way. Figure 3a shows that applying a right triangle with catheti a and b, and a string of length $l = 2a$, a similar oval will be produced whose arcs have the radii $l = 2a$ and $r = 2a - \sqrt{a^2 + b^2}$. Obviously, since a and b have to satisfy the relation

$$a \leq \sqrt{a^2 + b^2} \leq 2a,$$

the length b must be

$$0 \leq b \leq a\sqrt{3}.$$

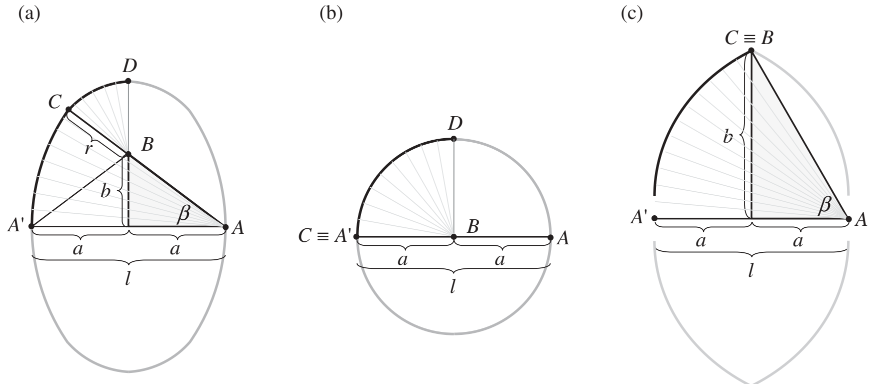

Figure 3. (a) The generalized Egyptian oval; (b) the extreme case β = 0°; and (c) the extreme case β = 60°.

The case $b \rightarrow 0$ means that the oval degenerates into a circle with a radius a (Figure 3b). The other extreme, i.e., $b \rightarrow a\sqrt{3}$, gives the greatest possible deviation from the circle, however, this is not a smooth curve any more (Figure 3c), so this extreme cannot be considered as an oval. (The analyzed groundplans in Section 4 varied between these two extremes.)

The deviation from the circle can be characterized by the eccentricity angle β shown in Figure 3a: $\beta = 0$ corresponds to the circle, while the other extreme is $\beta = 60°$ (Figure 3c) for which the smaller radius r vanishes.

The groundplans of all domes analyzed in the present paper were generalized Egyptian ovals. The area of the plan was the same in all cases, while they differed in their eccentricity angle β. The aim was to investigate the effect of the deviation from the circle on the minimal thickness of the dome.

Ovals can be constructed in several other ways. One possibility—often seen in Gothic architecture—is to place the basic point A outside the curve (see Figure 4). Such a solution was applied in certain historical structures (see Huerta (2007) citing, e.g., Koepf (1969), Bucher (1972), or Vandelvira (1580)). Other possibilities arise when more than two different arcs are used to compose the oval; or different construction methods of ellipses are applied, etc. However, the present investigation is restricted to the most prevalent versions, i.e., the generalized Egyptian ovals only.

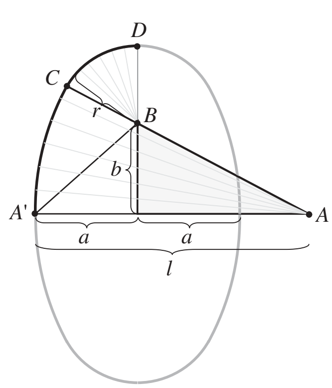

Figure 4. Oval with A positioned outside the curve.

2.2. The surface of the intrados

After drawing the groundplan, the builders of a dome had to define the 3D geometry of the internal surface ("intrados") in order to prepare the centering for the voussoirs, or—in case the dome was to be built without centering—a light guiding scaffold to prescribe the geometry of the intrados. According to Huerta (2007), the most common solution was to define the intrados as a surface of revolution, being rotated either about the longer axis of symmetry of the plan (e.g., San Andrea del Quirinale), or about the short axis (e.g., Cesarean Library in Vienna). In the present study both possibilities were considered (see Figure 5): the first option will be referred to as Type 1 surface ("flat" domes), while Type 2 will denote the second option ("high" domes).

2.3. The complete dome

Now the 3D body of the dome is, in principle, easy to define mathematically: from every point of the intrados, perpendicularly to the surface, the uniform thickness has to be measured outwards, to receive the points of the extrados. In the DEM simulations the task is more complicated: the continuous domain between the intrados and extrados has to be constructed as a collection of 3D brick-like discrete elements the length, l, and height, h, of which are aimed to be approximately equal along the complete dome, and their thickness t to be uniform. This was achieved in the 3DEC models in the following way.

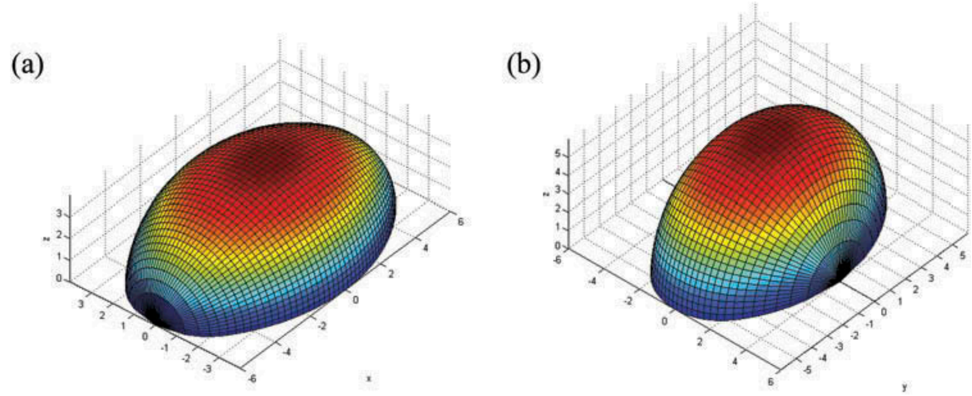

Figure 5. The intrados as a surface of revolution: (a) about the longer axis, Type 1 (flat) dome; and (b) about the shorter axis, Type 2 (high) dome.

Since the intrados is a surface of revolution, its sections perpendicular to the axis of revolution are circular arcs. The composition of the discretized model of a dome starts by considering the circular arc with the largest radius perpendicular to the axis of rotation. This arc is shown in Figure 6. Obviously, R_{int} is the half of the other axis of the plan being perpendicular to the axis of revolution. Measure the desired brick height, h, starting from the lowest point of the arc proceeding upwards as many times as wanted. (An opening for an oculus may be left out at the top in the model, while if such a hole is not desired, the small domain, where a full brick height cannot be placed, will be filled at the end of the construction procedure by a single closing element.) Through each point received this way (see the dark dots in Figure 6), imagine a horizontal cutting plane. The intersection of the i-th plane with the intrados will serve as the i-th "master curve," i.e., the basis of preparing the i-th horizontal ring of discrete elements. (Note that the master curves are not similar to each other.)

Figure 7 shows how the inner-lower sides of the elements are placed along the master curve. The process starts at a randomly chosen point, P_1. The brick length, l, should be measured along the curve, as many times as possible. However, this way the master curve is not followed smoothly by the brick elements, and it may lead to sharp corners particularly in those parts of the dome where the curvatures are high. Thus, the curvature of the master curve is taken into account in the algorithm by dynamically changing the brick length along the curve as shown in Figure 7 (imitating a mason who uses smaller stones for the strongly curved parts of the structure). Finally, truncated or elongated lengths are applied to close the ring, similarly to real masonry constructions.

The k-th discrete element of the ring is formed with the help of its two already existing nodes, P_k and P_{k+1}. By measuring the uniform thickness perpendicularly to the intrados in the outwards direction, two additional nodes are received. The intersection of the plane being perpendicular to the master curve in point P_k with the i+1-th master curve and a similar intersection point of the perpendicular plane at P_{k+1} with the i+1-th master curve will give two more nodes. From these two new nodes the thickness is measured outwards again to get the two missing nodes of the k-th element. (Note that the angles determined by the edges of such an element slightly deviate from being perpendicular.) After finishing the ring, a next layer can be prepared in a similar manner.

Since the master curve is horizontal and the top faces of the blocks forming a ring are determined by the outwards normal vector sweeping along the master curve, the union of the top faces is not planar. Consequently, in a

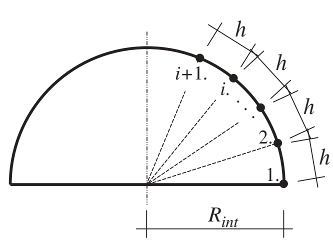

Figure 6. Largest vertical cross-section perpendicularly to the axis of rotation: definition of the vertical positions of the master curves.

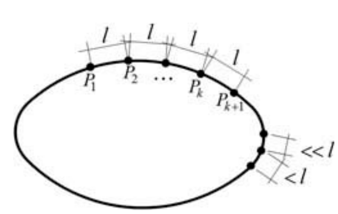

Figure 7. Horizontal view: The i-th master curve, with dynamically shortening brick lengths where the curvature is large.

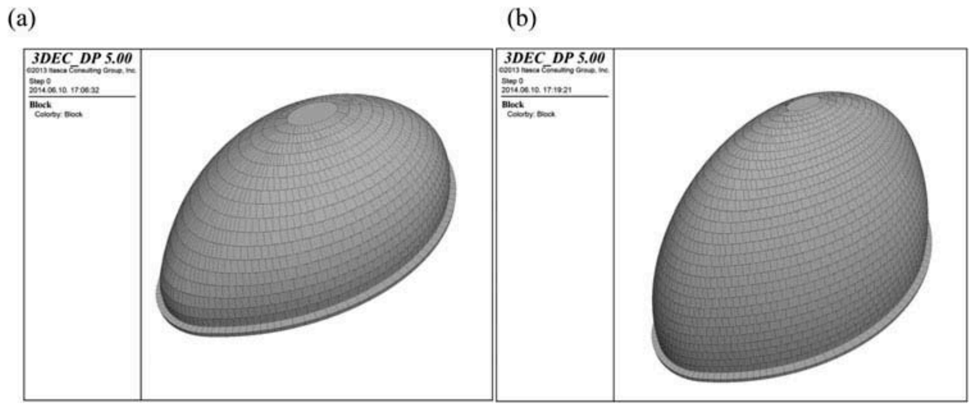

Figure 8. Discrete element model of the geometry of: (a) a Type 1 and (b) a Type 2 dome based on a generalized Egyptian oval (β=50°).

mathematical sense, the bottom corners of the next ring of blocks do not perfectly fit to the top of the blocks below them. However, the discrepancy was found to be negligible for those dimensions applied in the simulations, near the range of numerical rounding errors, hence it did not make any mechanical effect.

Similarly to real masonry structures, truncated or slightly elongated elements are applied not only to close the horizontal rings of voussoirs but also to avoid having interstices just above each other.

Figure 8 shows two geometrical models constructed in the above manner: a generalized Egyptian oval with $\beta = 50°$ is applied to generate a Type 1 and a Type 2 dome.

Finally, a remark has to be made on the issue of using uniform thickness in the applied geometrical models. In many real domes, especially of largish radius, the thickness is not uniform along the meridian: smaller around the top and larger near the bottom. This change in thickness results in a specific distribution of loads along the meridian, and can make the dome more stable. Consequently, the results in this article can be considered as a conservative approximation of the behavior of domes with varying thickness.

3. Numerical modeling issues

3.1. 3DEC

The commercial DEM code 3DEC was applied in the simulations. UDEC ("Universal Distinct Element Code"), the 2D ancestor of 3DEC, was originally developed for the modeling of fractured rocks (Cundall, 1971), but today its 2D and 3D versions are widely used in the engineering practice also for masonry structures.

The discrete elements in 3DEC may have any polyhedral shape, and may either be perfectly rigid, or they can be made deformable in such a way that they are divided into simplexes (tetrahedra in 3D) which serve as uniform-strain finite elements. This article applied perfectly rigid elements. In this case each rigid element has a reference point whose displacements (translations and rotations) during a small finite Δt time interval are determined with the help of Newton's laws of motion, taking into consideration the inertia of the whole element. Forces acting on the elements may be either external loads or exerted by the neighboring elements through the joints. The mechanical model of the joint behavior is a crucial issue, and will be discussed in Section 3.2 in detail. An explicit time integration scheme, based on central differences, is used for simulating the mechanical behavior (motions, changes of contact forces, etc.) over time: the simulation of the state changing under a given loading process is achieved by step-by-step calculation of the motions of the reference points.

3.2. Calibration: Simulations of spherical domes

3.2.1. Introductory remarks

The key of composing a reliable discrete element model for a structure is the careful calibration of the model properties, i.e., the necessary numerical parameters as well as those controlling the numerical time integration, method of loading, boundary conditions, etc. The model properties in the present study were calibrated with the help of the analysis of Heyman's original problem, i.e., a hemispherical dome being cut into orange-slice-like partitions (see Figure 9). The following characteristics had to be suitably set so that the minimal wall thickness would be the same as that of Heyman:

(i) **Contact parameters**. The contacts in all simulations were frictional which means that the following three contact parameters had to be chosen properly. The normal stiffness ("penalty

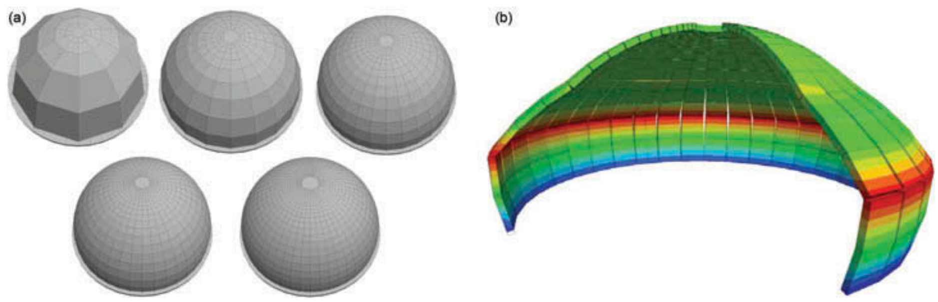

Figure 9. Calibration of the element size: (a) The analyzed densities; (b) collapse of a 50-segment spherical dome (colors indicate displacement magnitude).

stiffness," k_N) expresses how difficult it is to press the boundary point of an element into the interior of its neighbor: it is the intensity of the distributed compression force occurring at unit depth of the penetration between the two elements. The second parameter, the shear stiffness of the contact, ensures that when a slight relative displacement increment occurs in the tangential direction between two blocks, a tangential force —equal to the displacement increment times the tangential stiffness—arises in the opposite direction, and prevents the contact from unrestricted sliding. The third parameter is the coefficient of the classical Coulomb-friction.

The joints between the elements in a DEM model may have different physical meanings. The joints may represent some kind of mortar layer (or, e.g., clay layer in fractured rocks) having a finite thickness in reality between deformable blocks representing the voussoirs. If using perfectly rigid discrete elements (like in the present study), the joints in the model should also reflect the deformability of the voussoirs: in this case the material parameters of the joints express the total deformability of the blocks–and–joints system, therefore a normal and a tangential stiffness have to be properly verified along with either some fracture criteria (normal and shear strength) and/or a friction coefficient in order to define the conditions when the joints fail. In the present study the friction coefficient gave the only limit for the failure of the contact, and no fracture criteria were applied.

Note that for dry joints between blocks having irregular (nonsmooth) surfaces the material parameters of the joints should also include the possibility of the contacting blocks to get closer to each other under large pressure and to resist tangential relative translation due to the shear resistance of the small irregularities on the contact surface. Since these phenomena related to nonsmooth surfaces are too complex, their quantitative analysis was not considered in the present study.

From a computational point of view, the larger are the applied contact stiffnesses in a model, the smaller is the maximally allowed time step in the explicit solver, so the calculations become more time-consuming with increasing stiffnesses. On the other hand, too low stiffnesses may lead to unrealistic results: the contacting voussoirs may significantly penetrate into each other leading to a global mechanical behavior similar to a collection of soft blocks, and may even cause the numerical collapse of the simulations, while a rigid-block system with increasing stiffness tends to the theoretical model of Heyman's classical theory. So in the calibration tests special attention was paid to find the regime of contact penalty parameters for which the behavior is already acceptable regarding convergence to Heyman's classical results to the accuracy intended to reach. The results were then compared to mortared joints with realistic elastic characteristics. These tests are introduced in Section 3.2.2. The second parameter, the tangential stiffness, k_S, was chosen to be 1/10 of the normal stiffness.

The third parameter, the friction coefficient (f), should be infinitely large according to Heyman's conditions. In the calibration tests where the aim was to reproduce Heyman's results the friction angle was indeed set to 90°.

After the calibration tests, in the analysis of oval domes in Section 4, Coulomb friction with $f = 0.7$ was applied first. Then coefficients ranging from 0.3–0.7 were considered to carry out sensitivity analysis regarding the contact properties. Finally, friction coefficient was decreased further, with very small steps (determining the minimal wall thickness for each value), to find that value for every intrados where the purely hinging collapse mechanism turned into a combined hinging-sliding mode for insufficient wall thickness, and that value where the mixed collapse mechanism turned into pure sliding failure mode so that the structure was unable to equilibrate its weight with any wall thickness.

(ii) **Element size**. The elements in a DEM model may either directly correspond to the individual voussoirs, or each element models a collection of several bricks or stones. While the computational time decreases with the decreasing number of elements, due to the bending resistance of the individual blocks the overall load bearing capacity of the structure may be overestimated if the subdivision is not dense enough. So it was also an open modeling issue how densely a dome should be divided into discrete elements. Section 3.2.2 deals with this question as well.

(iii) **Loading technique: method of de-centering**. In a DEM simulation the gravity can either be “switched on” in a single step (as if dropping the self weight suddenly on the whole structure), or the structure can initially be fixed at all nodes while the gravity is already acting and then the nodes are gradually released, starting from the top and proceeding downward in several steps, finding the equilibrium in each step before releasing the next set of nodes (as if decentering a real dome). With a series of calibration tests it was checked whether the difference in the loading technique made an influence on the results. Details will be given in Section 3.2.3.

(iv) **Parameters controlling the numerical time integration**. Since the basis of the present study was to check whether different domes with given geometries can find their equilibrium state without collapse (hence the exact history of how the blocks find their equilibrium position is unimportant), in all tests the 3DEC default parameters for static analysis were applied: “auto” damping with a coefficient of 50% (half of the change of kinetic energy was dissipated in each time step), and the time step length offered automatically by 3DEC was accepted (see Itasca (2007) or Cundall (1982) for detailed explanations). Note that these parameters would not be suitable when simulating a dynamic process, e.g., earthquake analysis.

(v) **Boundary conditions**. The lowest elements of the domes were supported from below by a ring of perfectly fixed elements having the same contact parameters as those blocks forming the domes. So the lowest voussoirs of the domes had an elastic–frictional, Coulomb-type contact with this “foundation”.

3.2.2 Calibration of the element size and the contact normal stiffness

Figure 9a illustrates the analyzed geometries: the discrete elements were defined by slicing the dome volume by dividing its base perimeter into 10, 20, …, 50 sections, and applying the same density of discretization for each slice. Note that the vertical interstices between the elements are just above each other in the calibration tests, corresponding to the slicing technique presented by Heyman. This very special arrangement was applied only in the calibration tests where Heyman’s theoretical prediction was intended to reach; then in the simulations in Section 4 the vertical joints between stone blocks were always shifted with respect to each other.

For each geometry shown in Figure 9a, a sequence of different penalty stiffnesses was tried, and the minimally necessary wall thickness was determined for each penalty stiffness in the following way. For a given middle surface, k_N and density of subdivision, several different domes were prepared which differed only in their wall thickness. Unlike in the simulations of oval domes (whose geometry were prepared according to the method explained in Section 2), for the calibration tests the middle surface of all domes was the same hemisphere with unit radius R, in order to follow Heyman’s analysis as closely as possible. Half of the thickness was measured outward and the other half was measured inwards along the normal vector of the middle surface. The applied thicknesses differed by 0.1% of the middle radius, e.g., $t = 0.039\ R$, $0.040\ R$, $0.041\ R$, etc. were applied. Then for every case the selfweight was put on the dome, time stepping was started, and continued until either collapse or finding a balanced state. The collapse was recognized by monitoring the vertical displacements of the closing element on the top of the structure. If this displacement was greater than 5% of the height of the dome, collapse was recognized and the simulation stopped. On the other hand, balanced state was validated by checking the displacement and velocity of the closing element on the top of the dome and also the unbalanced forces in the system. The balanced state was assured under the following condition: the displacement, velocity and unbalanced force had to be lower than 10^{-6} m, 10^{-7} m/s and 10^{-5} N, respectively. To illustrate this, Figure 9b shows the collapse mechanism for the 50-segment dome with a thickness slightly under the critical value: the perfectly axisymmetric geometry of the collapse mechanism can clearly be observed.

Finally, the smallest thickness for which the dome did not collapse was selected; this thickness is shown on the vertical axis of Figure 10. The thickness is normalized with the radius of the middle surface R. The results show that as the contact stiffness and subdivision density increase, the minimal thickness tends to Heyman's prediction. The stiffness value $k_N = 10^{11} - 10^{12}$ N/m^3 and subdivision of the perimeter into 30 sections (brick length $l = 0.209\ R$) are already sufficient to get a good agreement with Heyman's result: the minimal thickness for which the domes did not collapse approached 0.042 times the radius of the middle surface. Based on this, the characteristic length of the bricks applied in the simulations in Section 4 were around 40 cm ($l = 0.08\ R$), which is close to realistic sizes, and definitely smaller than what would be necessary to capture Heyman's result on minimal wall thickness of spherical domes.

Real contacts and real voussoirs have finite stiffnesses, consequently according to the results shown in Figure 10, real domes require bigger thickness to be stable than predicted by Heyman's rigid block theory. However, the results also show that if the subdivision is dense enough (i.e. the perimeter is subdivided into at least 30 elements), then for k_N being above 2 GPa/m the minimal wall thickness does not significantly differ from Heyman's prediction: it remains under 105% of the theoretical value, and decreases with increasing k_N. For k_N being above 10 GPa the difference is negligible. So the question is what is the realistic range of joint stiffness. To approximate this range, consider two blocks shown in Figure 11a, both having the same thickness l_b = 0.40 m, and a mortar layer of l_m = 1.5 cm (the two contact surfaces have unit area). Assuming unrestricted crosswise extension, the k_N joint stiffness of the equivalent rigid block—deformable joint—rigid block system is

$$k_N = \frac{E_b E_m}{l_b E_m + E_b l_m},$$

where E_b and E_m denote the Young-modulus of the block and the mortar respectively. Typical Young-moduli E_b are between 5 GPa (shale or mudstone) and 100 GPa (exceptionally stiff marble or granite). For mortar E_m = 1 – 5 GPa can be estimated. The equivalent joint stiffness for the very small values E_b = 5 GPa and E_m = 1 GPa becomes k_N = 10,53 GPa/m for which the minimal wall thickness is 102% of Heyman's prediction; for more realistic Young moduli the equivalent joint stiffness is an order of magnitude higher so the deviation from Heyman's prediction is negligible. (For instance, for marble and a stronger mortar, E_b = 50 GPa and E_m = 2 GPa, the equivalent stiffness becomes k_N = 64,52 GPa/m, for which Figure 10 shows that the deviation from Heyman's prediction is negligible.) Note that for restricted crosswise deformations the equivalent stiffness becomes higher because of the Poisson-effect, and dry contacts can probably be approximated with even higher k_N than mortared joints, around 10^{11}–10^{12} Pa/m. Similar values for k_N were also found in discrete element simulations of two deformable blocks with a third discrete element between them representing a mortar layer between the two voussoirs, submitted to compression as shown in Figure 11b. Different Young-moduli, Poisson ratios, and friction coefficients were tried for both unrestricted and restricted crosswise deformations. The simulation results confirmed the above values for k_N.

3.2.3. The role of the loading method

Construction with centering was simulated and tested in the following way. Two spherical domes were prepared with the same intrados and a chosen thickness (the arrangement of the discrete elements was realistic now,

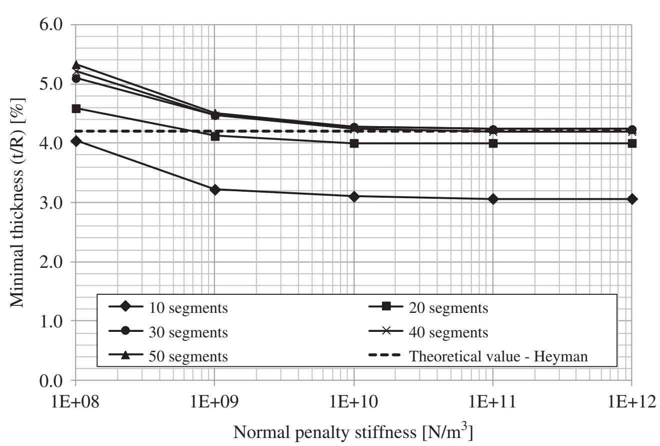

Figure 10. Dependence of the minimal wall thickness on the density of subdivision and on the contact penalty stiffness for orange-slice-like spherical domes.

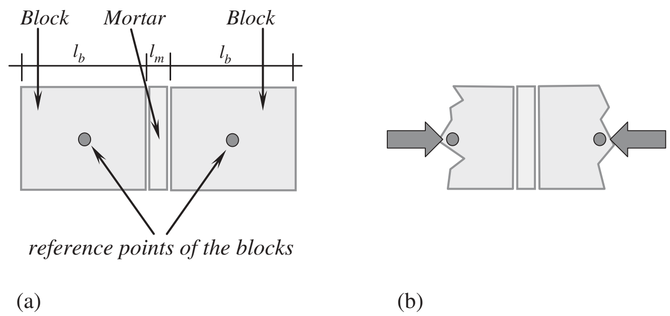

Figure 11. Mortared joint between deformable blocks: (a) geometry of the block – joint – block system; and (b) the system submitted to compression.

i.e., the elements were of the same size apart from those few which had to be truncated, so that the interstices were not above each other). At the beginning, the gravity was already acting while all nodes of the elements were still fixed against translations. Then in the first case the elements were gradually released starting from the top of the dome and proceeding downwards, as if removing a centering, in ten consecutive steps. The structure was equilibrated after every step. For the other dome the whole centering was removed (all the elements were released) in one single step. Using the same intrados with several different wall thicknesses, the minimally necessary thickness was then determined for each case in the same manner as explained in Section 3.2.2.

The results on the minimal thickness showed no noticeable differences between the different de-centering techniques. So the simplest possible technique can reliably be used in the computer simulations, hence the rest of the tests were done by decentering the domes in a single step. It is important to emphasize, however, that this statement has been checked only for the loading case which is relevant for the present study, i.e., only for pure self-weight. In other problems where the effect of a gradually increasing live load is analyzed special attention has to be paid if an adaptive global damping technique is used: the damping parameter has to be returned to the original high value before a new load increment is applied.

4. Simulation results

4.1. The analyzed domes

The applied ground plans are shown in Figure 12; their deviation from the perfect circle is quantified with the help of the eccentricity angle β (see Section 2.1). All ground plans had equal internal area, the same as that of a circle with a 5 m radius (i.e., the equivalent inner radius, R_{eq}, was 5 m for each oval). (Note that the ratio of minimal thickness to inner radius does not depend on the actual radius size, except that the penalty

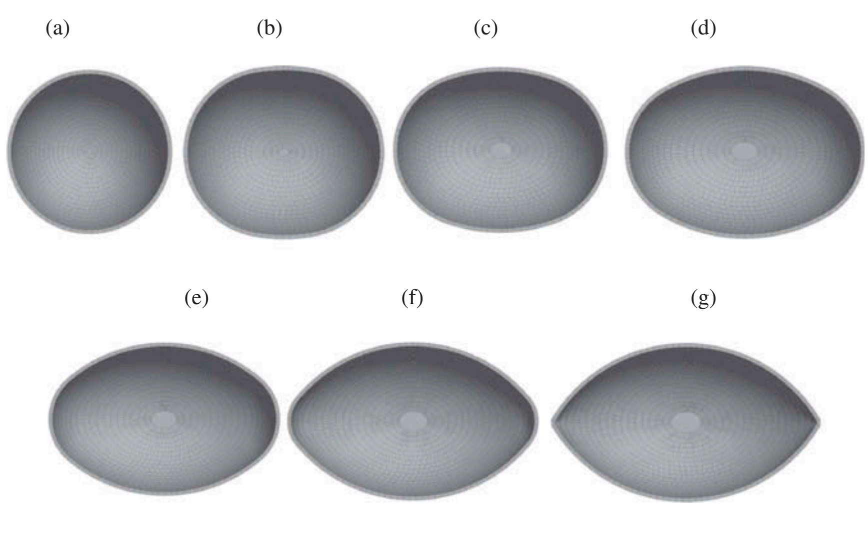

(a) $\beta = 0$; *(b)* $\beta = 10°$; *(c)* $\beta = 20°$; *(d)* $\beta = 30°$; *(e)* $\beta = 40°$; *(f)* $\beta = 50°$; *(g)* $\beta = 60°$

Figure 12. Ground plans of the analyzed domes.

stiffness should be recalibrated if the size of the dome (thus the internal forces) change with orders of magnitude in comparison to the calibrated model.)

Rotating each groundplan about its longer or shorter axis of symmetry, a Type 1 or a Type 2 intrados was received, respectively. Then—according to the method described in Section 2.3—several complete domes were constructed for each intrados, differing in their wall thicknesses but covering the same net area. (This means that the area of the groundplan defined by the intrados was the same in every model, but the equivalent radius of the middle surface also increased with the thickness.) The characteristic lengths for the definition of the elements were

$l = 0.40$ m

$h = 0.40$ m

and the thickness, t, was changed from simulation to simulation in steps of 0.1% of the equivalent inner radius R_{eq}.

For every geometry the material density 2500 kg/m^3 and the usual gravitational acceleration, 9.81 m/sec^2 was applied in the calculation of the weight of the blocks. The same contact characteristics were used in every model: normal stiffness $k_N = 10^{12}$ N/m^3, tangential stiffness $k_S = 10^{11}$N/m^3.

4.2. Results for f = 0.7 friction coefficient

Since most of the constructional stones and bricks have at least or about this frictional capacity, for every intrados the minimal wall thickness was first determined for 35° friction angle (0.7 friction coefficient). Figure 13 summarizes the most important results. The horizontal axis measures the eccentricity with the angle β: the deviation from the circle increases from left to right. The vertical axis shows the minimally necessary thickness, t_{min}, normalized by R_{eq}, and expressed in [%].

In the case of a circular ground plan and rigid elements $t_{\min} = 0.037\ R$ was received, smaller than the value 0.041 found by Lau (2006) by taking into account hoop resistance. The result naturally differed from the outcome of the calibration tests and Heyman's result: those domes in the calibration and in Heyman's derivation had an orange-slice structure, while the analysis in Section 4 was based on realistically, irregularly arranged voussoirs where the frictional resistance on the horizontal contact surfaces and the tension resistance of the individual blocks provided a hoop resistance. This is explained in Figure 14: the separation of the two blocks in the middle ring is encumbered by the frictional forces expressed by the upper and lower blocks. A possible explanation of the deviation from Lau (2006) is suggested by the characteristic collapse mode shown in Figure 10 for the orange-slice-like arrangements and also found for the realistically placed voussoirs. Unlike in the case of the continuum model applied by Lau (2006), in a DEM model the tangential stiffness k_S is finite so the elements may slightly translate elastically along each other in the plane of the contact, even without frictional sliding. The typical collapse mechanism of a hemisphere includes that the lowest part of the dome rotates outwards about the external perimeter of the groundplan (again, see Figure 10). A slight outwards translation of the lowest blocks shifts this external supporting ring of hinges into a more favorable position, and contributes to the resistance against collapse.

The results in Figure 13 show that with significant deviations from the spherical shape, the minimum thickness differs only 25% of the value required for a hemispheral

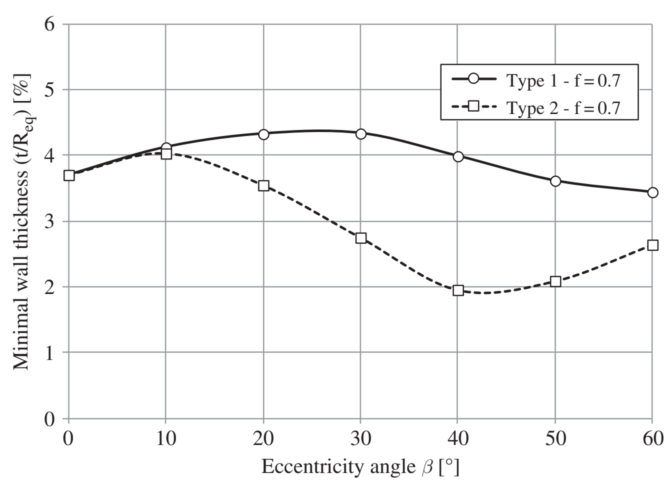

Figure 13. The necessary minimal wall thickness normalized by the equivalent radius (expressed in %) as the function of the eccentricity of the groundplan.

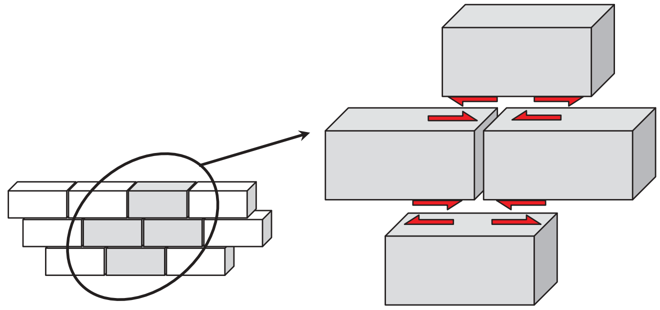

Figure 14. Explanation of hoop resistance: red arrows represent frictional forces, not allowing the blocks of the middle layer to separate.

dome with the same net groundplan area in case of Type 1 (flat) domes, but this difference can be as high as 50% if the results of the Type 2 (high) domes are considered.

Type 2 ("high") geometry appears to be more favourable from mechanical point of view than a spherical intrados: apart from the range of nearly circular ground plans, smaller wall thickness is sufficient to balance the own weight of the structure. This is not the case for the Type 1 geometries: the necessary wall thickness is greater for oval ground plans than for a spherical dome except for domes with very high eccentricity. This difference may be explained by the fact that in case of Type 2 geometries the longitudinal cross sections are half-circles and the transverse cross-sections are vertically elongated ovals (somewhat resembling to a pointed arch); for Type 1 geometries the transverse cross sections are the half-circles and the longitudinal cross-sections are horizontally elongated ovals whose resistance against the self weight is poorer.

Figure 15 shows the total volume of the elements assuming that the minimal wall thickness is applied everywhere. The horizontal axis measures the eccentricity β again. For medium to large eccentricities (β = 20°–55°) Type 2 domes are more favourable in the sense that they require less building material than either the spherical or the Type 1 domes; however, in the case of extreme eccentricity (β = 60°) Type 1 domes need the smaller amount of masonry.

It is interesting to compare how the Type 1 and Type 2 domes collapse if their wall thickness is too small. For low eccentricities the collapse mechanisms are similar to that of a hemisphere (see Figures 16a and 16b): two intermediate rings of hinges form the lower of which moving outward, the upper moving inward. The rings are not perfectly horizontal: in all cases they slightly descend towards the two ends of the longer axis. As the eccentricity increases, a characteristic difference can be noticed between the collapse mechanisms. A Type 1 dome is a flat, elongated structure: in this case the rings of hinges deviate more and more from the horizontal plane with increasing eccentricity, and a kind of bulge can be noticed where the outwards ring approaches the base level near the narrow ends of the oval base (see Figure 17a). The collapse of Type 2 domes with large eccentricities happens in nearly the same way (Figure 17b), the only difference is that since

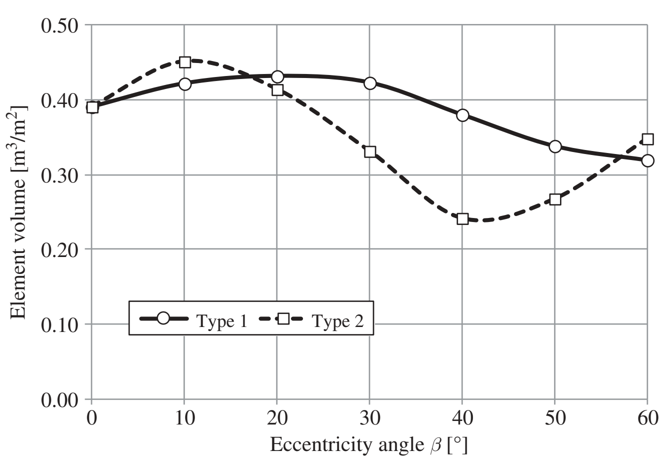

Figure 15. Total volume of masonry normalized with groundplan area when applying the minimally necessary thickness, expressed in m^3/m^2 on the vertical axis, as the function of the eccentricity of the groundplan.

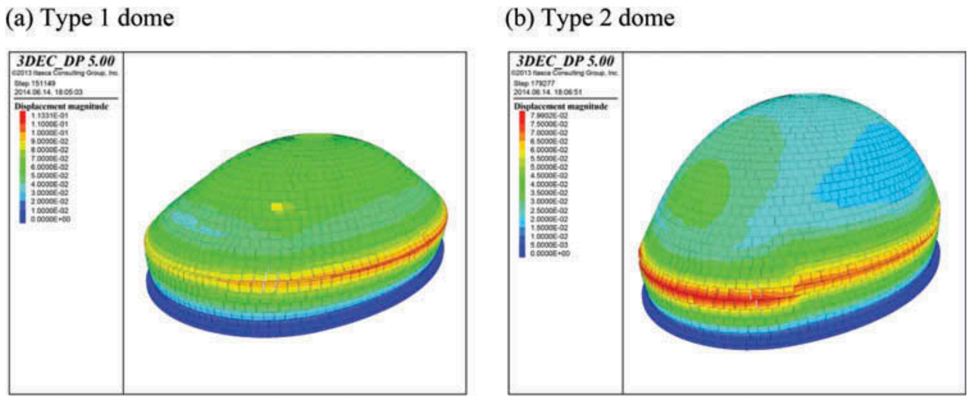

Figure 16. Hinging collapse modes: (a) Type 1 (flat) dome and (b) Type 2 (high) dome, both with β = 30° ground plan (color scale indicates displacement magnitude).

the strongly curved parts of the dome form a relatively rigid vertical circular arch-like strip overarching between the two sharp ends of the groundplan above the longer axis of symmetry, such a bulge like the one seen in Figure 17a cannot occur and the lower parts of the strongly curved arch-like strip simply buckle outward.

Domes are often built with an oculus, i.e., a round opening (circular or oval) around the top of the dome. For spherical domes a small circular oculus does not influence the minimally necessary wall thickness according to Heyman's theory, and the same can be expected for oval domes with small eccentricities. To analyze the question, additional simulations were done for the same intrados geometries as before, but with an oculus of the size 10% of the longer axis of the groundplan, and checked the collapse modes for f = 0.7 and slightly insufficient wall thickness. The only difference could be detected in the collapse modes of Type 2 domes with large eccentricities (see Figure 18). A Type 2 structure becomes higher with increasing eccentricity; the vertical circular ach-like strip becomes more and more dominant along the longitudinal cross section, and the two sides of the dome flatten out as their surface curvatures decrease. For eccentricities about $\beta >$ 45° the failure was initiated by the flattened parts falling inwards because of their low resistance for bending and because of the missing part of the masonry shell around the top (Figure 18).

4.3. The effect of contact friction coefficient

In order to analyze the effect of frictional resistance on the minimal wall thickness and collapse modes, every intrados applied in Section 4.2 was simulated with several different friction coefficients and wall thicknesses. The simulation results are summarized in Figure 19. Every line in the diagram belongs to a specific intrados, and shows how the minimal wall thickness depends on the value of the friction coefficient f between the voussoirs. (The minimal wall thickness is normalized by the equivalent radius R_{eq}.) Collapse modes of the domes with t being slightly

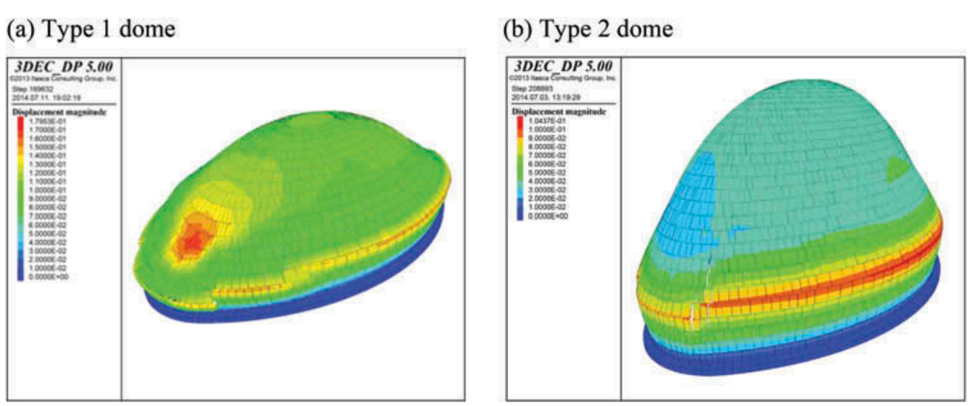

Figure 17. Hinging collapse modes: (a) Type 1 (flat) dome and (b) Type 2 (high) dome, both with β = 50° ground plan (color scale indicates displacement magnitude).

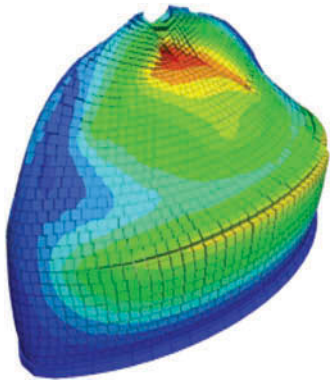

Figure 18. Hinging collapse mode of a Type 2 (high) dome with an oculus, with β = 55° ground plan (color scale indicates displacement magnitude).

below the minimally necessary value were also observed. According to the experiences, three domains of the friction coefficient can be identified for each intrados.

(1) For f above approximately 0.2–0.3 the minimal wall thickness is not sensitive to f in the observed range (up to f = 0.7). In these cases collapse occurring for insufficient wall thickness happens with a hinging mechanism, without sliding. The lower boundary of this domain of f, the transitional friction coefficient f_{tr}, depends on the geometry of the intrados.

(2) Below f_{tr} but above the value of critical friction coefficient f_{cr}, a combined collapse mode containing sliding and rotational hinging occurs if the wall thickness is too small. Such a collapse mode can be seen in Figure 20a for a Type 1 dome and in Figure 20b for a Type 2 dome. In this range the value of $t_{\min}$ strongly depends on f. The smaller is the friction coefficient, the larger is the necessary wall thickness to balance the self weight, and sliding becomes more and more dominant in the collapse mechanisms.

(3) Below the f_{cr} critical friction coefficient belonging to the analyzed intrados, the structure cannot be in equilibrium for any thickness. In this case a pure sliding mechanism can be observed. Failures of this type are shown in Figures 21a and 21b.

These three domains were also found by D'Ayala and Casapulla (2001) for hemispheral domes with finite friction. While for Heyman's orange-slice-like cracked domes the two special values of f separating the three domains are f_{cr} = 0.20 and f_{tr} = 0.25 in the DEM simulations, according to their theory D'Ayala and Casapulla (2001) found that for membranes with fixed supports against any translation, and considering their "x+z" curve which corresponds to removing a fictitious constraint on the position of the thrust surface, their values were 0.136 and 0.25, respectively. For the hemispheric dome with brick ordering providing hoop resistance 0.20 and 0.23 is given by the DEM simulations (For semicircular arches the same three domains were recognized and determined by Sinopoli et al. (1997) and Gilbert et al. (2006), with the separator values f = 0.31 and 0.395. The existence of the three collapse modes was also confirmed by the discrete element simulations of Rizzi et al. (2014) for different arches.)

Figure 22 summarizes the f_{cr} and f_{tr} values depending on the eccentricity of the groundplan. The critical friction values (two curves with solid markers) indicate that Type 1 ("flat") domes are more sensitive to sliding failure, while in the case of Type 2 ("high") domes the critical friction coefficients are always lower than that of the spherical dome (which was found in the present study to be approximately 0.20). The highest and lowest critical friction coefficients are 0.24 (for Type 1) and 0.14 (for Type 2), and both values were obtained at very high eccentricity (angle β around 50°). The two curves with the empty markers represent the transitional friction coefficient. For a hemisphere it was 0.23 and for different oval shapes its value varied between 0.31 and 0.16.

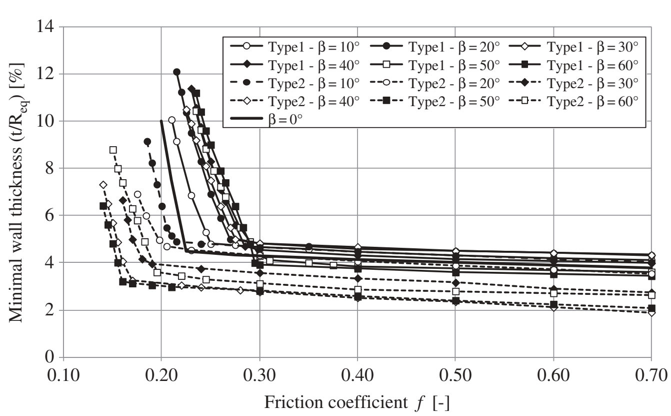

Figure 19. The necessary minimal wall thickness normalized by the equivalent radius (expressed in %) as the function of the applied friction coefficient (solid lines: Type 1 domes; broken lines: Type 2 domes).

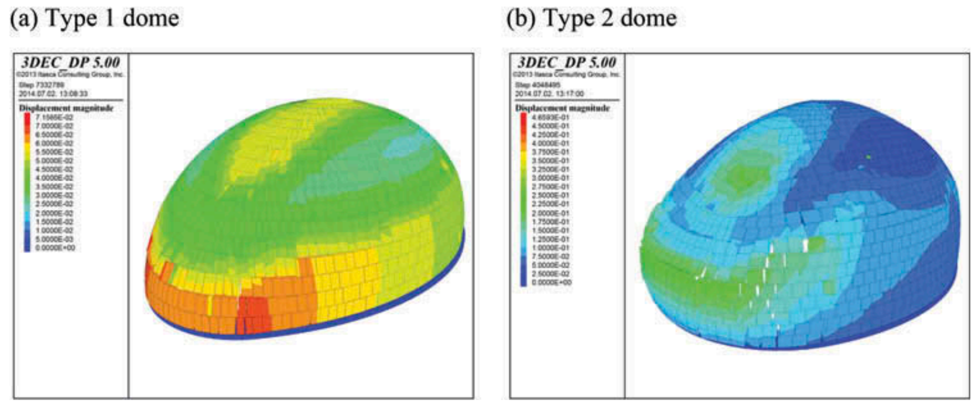

Figure 20. Mixed collapse modes: (a) Type 1 (flat) dome with β = 50° ground plan and (b) Type 2 (high) dome with β = 30° ground plan (color scale indicates displacement magnitude).

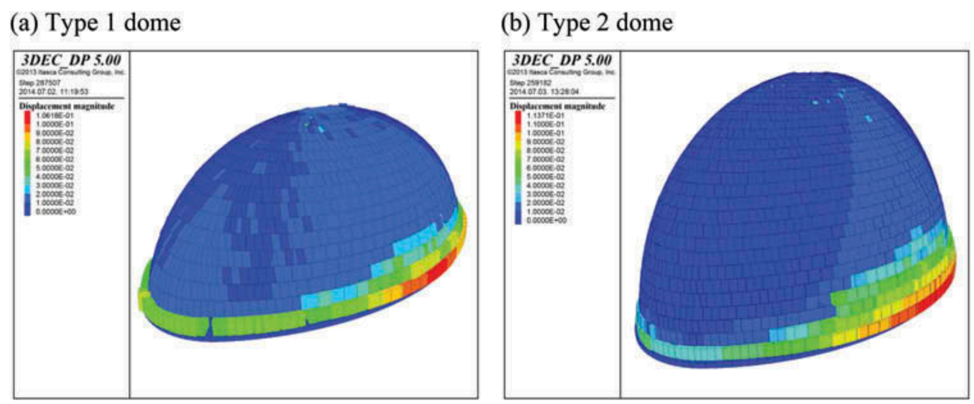

Figure 21. Sliding collapse modes: (a) Type 1 (flat) dome and (b) Type 2 (high) dome, both with β = 50° ground plan (color scale indicates displacement magnitude).

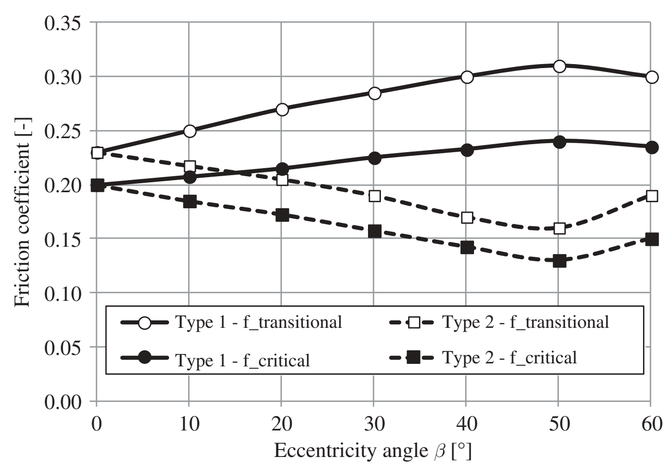

Figure 22. Critical and transitional frictional coefficient as the function of the eccentricity of the groundplan.

Consequently, if the friction coefficient is above approximately 0.3, every dome is in the range of purely rotational hinging collapse modes, and tendencies similar to those observed in the case of 0.7 friction coefficient can be recognized. This can be seen in Figure 23, where the minimal wall thickness (normalized by the equivalent radius) as the function of the eccentricity angle β is shown for different friction coefficients ranging from 0.3–0.7. Curves belonging to Type 1 domes with different friction angles (circular markers) are similar to each other. They indicate that slightly eccentric domes need higher thickness, and very

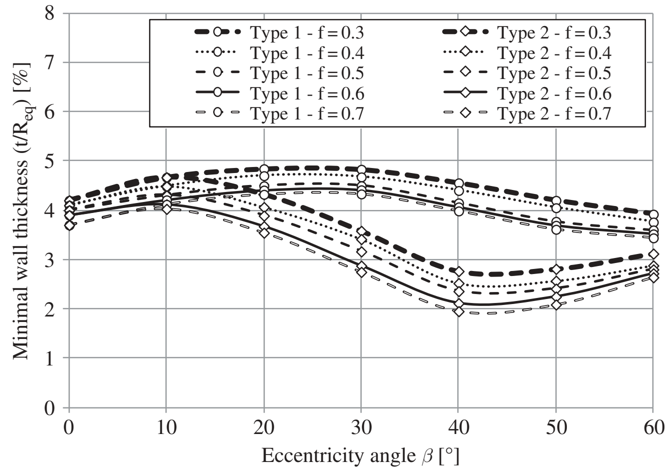

Figure 23. The necessary minimal wall thickness normalized by the equivalent radius (expressed in %) as the function of the eccentricity of the groundplan.

eccentric Type 1 domes are more favourable than spherical or slightly eccentric Type 1 domes. The curves belonging to the Type 2 domes (diamond markers) are also similar to each other; they show that domes with large eccentricities need smaller wall thickness than spherical or slightly eccentric Type 2 domes.

Since the friction coefficient can safely be assumed well above 0.3 in all practical situations (apart from very special extreme cases), the diagrams in Figure 23 offer a possibility for the practicing engineer to assess the geometrical safety of an actual oval dome. The thick broken lines (the upper and the lower of which belonging to the Type 1 and to the Type 2 domes, respectively) give a conservative estimation of the necessary wall thickness, depending on the eccentricity of the groundplan. This estimated minimal wall thickness can be compared to the actual thickness of the analyzed real dome to appraise the safety of the structure.

5. Conclusions

After a careful calibration procedure, several 3DEC simulations were done on dome models with different intrados shapes and wall thickness. The main advantage of using a discrete element code instead of developing an ad-hoc theoretical model like those in some of the quoted references is that the discrete element simulations could serve as virtual experiments: the history leading to failure or reaching the equilibrium could be followed with a step-by-step time integration scheme. The main disadvantage of using DEM is that the calculations are very time-consuming: on an average PC several hours may be needed for a given dome to collapse or to become equilibrated.

The following conclusions can be drawn from the results.

- In order to receive a close approximation of Heyman's classical theory with rigid blocks, the numerical control parameter k_N should be at least 10^{11}–10^{12} N/m^3 and the perimeter of the groundplan should be subdivided at least into 30 sections. (The value of k_N should be rescaled for model dimensions differing by orders of magnitude from those applied in this article.) Models with smaller k_N require slightly larger wall thicknesses to be stable; however, results based on realistic contact stiffnesses of mortared joints ($k_N = 10^{10}$–10^{11} N/m^3) differ only within a few percentage from the results belonging to theoretically infinite k_N. Domes with smaller k_N require larger wall thickness to be stable: the classical theory is slightly on the unsafe side.
- The simulations on hemispherical domes with rigid elements confirmed the conclusion of Lau (2006) that with hoop forces (caused by the frictional resistance along the horizontal joints) the minimal wall thickness is definitely smaller than suggested by Heyman. The discrete element simulations gave an even smaller minimum wall thickness than the value found by Lau: 0.037 times the radius was received for hemispheral domes. Note that this value was measured for 35° frictional angle (f = 0.7). In the analyzed range of the friction coefficient between $f_{tr} \leq f \leq 0.7$ the value of f only weakly affects $t_{\min}$.
- Type 1 oval domes need larger wall thicknesses than hemispherical domes except for geometries with very high eccentricity. On the other hand, apart from the region of low eccentricities (i.e., nearly

hemispheral domes) Type 2 domes can balance their weight with smaller thicknesses than hemispherical domes. Depending on the eccentricity of the groundplan, both Type 1 and Type 2 domes may require a lower total volume of masonry than a hemispherical dome to cover the same area.

- While in most cases it was found that for realistic frictional resistance the hinging failure mechanism was basically the same as for hemispherical domes, in the case of Type 2 domes having an oculus a new hinging failure mode was revealed for large eccentricities of the groundplan.
- For low frictional resistance (f being below f_{tr} whose value was found to be approximately 0.16–0.31 depending on the shape of the intrados), combined sliding-hinging collapse modes occur and the minimal wall thickness becomes strongly sensitive to f. Decreasing the frictional resistance even further, a critical value f_{cr} is reached which varies from 0.14–0.24, depending on the exact geometry of the intrados: at this critical value the necessary minimal wall thickness tends to infinity and a pure sliding failure occurs for any wall thickness.
- Conservative approximations on the necessary wall thickness were given in Figure 23 for the practicing engineer, to provide a tool for appraising the geometrical safety of an actual oval dome. After measuring the eccentricity of the groundplan and deciding whether the intrados has a Type 1 (flat) or Type 2 (high) geometry, the wall thickness of the analyzed real dome can be compared to the approximated necessary value.

Funding

This research was partially supported by the OTKA (Hungarian Research Fund) under grant no. 100770. Software 3DEC was provided by Itasca CG under the Education Partnership Program for which the authors also express their gratitude.

References

Alexakis, H., and N. Makris. 2013. Structural stability and bearing capacity analysis of the tunnel-entrance to the stadium of ancient Nemea. *International Journal of Architectural Heritage* 7 (6):673–692

Aoki, T., M.A. Chiorino, and R. Roccati. 2003. Structural characteristics of the elliptical masonry dome of the sanctuary of Vicoforte. *Proceedings of the First International Congress on Construction History*, ed. S. Huerta et al., Madrid, January 20–24, 2003.

Block, P., and J. Ochsendorf. 2007. Thrust network analysis: A new methodology for three-dimensional equilibrium. *Journal of the International Association for Shell and Spatial Structures* 48:167–173.

Block, P., L. Lachauer, and M. Rippmann. 2010. Validating thrust network analysis using 3D-printed structural models. *Proceedings of the IASS Symposium* November 8–12, Shanghai, China.

Block, P., and L. Lachauer. 2014. Three-dimensional funicular analysis of masonry vaults. *Mechanics Research Communications* 56:53–60.

Boothby, T.E. 2001. Analysis of masonry arches and vaults. *Progress in Structural Engineering and Materials* 3:246–256

Bucher, F. 1972. Medieval architectural design methods, 800-1560. *Gesta* 11 (2):37–51.

Cundall, P.A. 1971. A computer model for simulating progressive large scale movements in blocky rock systems. In *Proccedings of the Symposium of the International Society of Rock Mechanics*, Nancy, France, vol. 1, Paper # II-8.

Chappuis, R. 1976. Utilisation du tracé ovale dans l'architecture des églises romanes. *Bulletin Monumental* 134:7–36.

Cundall, P.A. 1982. Adaptive density-scaling fortime-explicit calculations. In *Proceedings of the 4th International Conference on Numerical Methods in Geomechanics*, pp. 23–26. Edmonton.

Cundall, P.A., and D.H. Hart. 1992. Numerical modelling of discontinua. *Journal of Engineering Computations* 9:101–113.

D'Ayala, D., and C. Casapulla. 2001. Limit state analysis of hemispherical domes with finite friction. In *Historical Constructions*, eds. P.B. Lourenco and P. Roca, Guimares, pp. 617–626.

D'Ayala, D.F., and Tomasoni, E. 2011. Three-dimensional analysis of masonry vaults using limit state analysis with finite friction. *International Journal of Architectural Heritage* 5 (2):140–171.

Fódi, A. 2011. Effects influencing the compressive strength of a solid, fired clay brick. *Periodica Polytechnica Civil Engineering* 55 (2), 117–128.

Gilbert, M., C. Casapulla, and H.M. Ahmed. 2006. Limit analysis of masonry block structures with non-associative frictional joints using linear programming. *Computers and Structures* 84 (13–14):873–887.

Heyman, J. 1967. On shell solutions of masonry domes. *International Journal of Solids and Structures* 2:227–240.

Heyman, J. 1969. The safety of masonry arches. *International Journal of Mechanical Sciences* 11:363–385.

Heyman, J. 1995. *The stone skeleton*. Cambridge: Cambridge University Press.

Heyman, J. 1999. *The science of structural engineering*. London: Imperial College Press.

Heyman, J. 2001. Why ancient cathedrals stand up. The structural design of masonry, *Ingenia* 10, Available at http://www.ingenia.org.uk/ingenia/issues/issue10/heyman.pdf.

Huerta, S. 2001. Mechanics of masonry vaults: The equilibrium approach. In *Historical constructions*, eds. P. B. Lourenco and P. Roca, Guimaraes: University of Minho.

Huerta, S. 2007. Oval domes: History, geometry and mechanics. *Nexus Network Journal* 9 (2):211–248.

Huerta, S. 2008. The analysis of masonry architecture: A historical approach. *Architectural Science Review* 51 (4): 297–328.

Huerta, S. 2010. Designing by geometry: Rankine's theorems of transformation of structures. In *Geometría y proporción* *en las estructuras. Ensayos en honor de Ricardo Aroca*, ed. R. Aroca. Lampreave, Madrid, pp. 262–285.

Isfeld, A., and N. Shrive. 2015. Discrete element modeling of stone masonry walls with varying core conditions: Prince of Wales fort case study. *International Journal of Architectural Heritage* 9(5):564–580.

Itasca Consulting Group 2007. *3DEC User's Guide*. Minneapolis, Minnesota.

Koepf, H. 1969. *Die gotischen Planrisse der Wiener Sammlungen*. Vienna: Hermann Böhlaus Nachf.

Lau, W.W. 2006. Equilibrium analysis of masonry domes. MSc Dissertation, Massachusetts Institute of Technology, Cambridge, Massachusetts.

Lawrence, J.D. 1972. *A Catalog of Special Plane Curves*, Dover, pp. 155–157.

Lemos, J.V. 2007. Discrete element modeling of masonry structures. *International Journal of Architectural Heritage* 1:190–213.

O'Sullivan, C. 2011. *Particulate discrete element modelling: A geomechanics perspective*. United Kingdom: Spon Press, Taylor and Francis.

Rizzi, E., F. Rusconi, and G. Cocchetti. 2014. Analytical and numerical DDA analysis on the collapse mode of circular masonry arches. *Engineering Structures* 60:241–257.

Sinopoli, A., M. Corradi, and F. Foce. 1997. Modern formulation of preelastic theories on masonry arches. *ASCE Journal of Engineering Mechanics* 123 (3):204–213.

Tóth, A.R., Z. Orbán, and K. Bagi. 2009. Discrete element analysis of a stone masonry arch. *Mechanics Research Communications* 36 (4):469–480.

Vandelvira, A. 1580. Exposición y declaración sobre el tratado de cortes de fábricas que escribió Alonso de Valdeelvira por el excelente e insigne architect y maestro de architectura don Bartolomé de Sombigo y Salcedo, maestro mayor de la Santa iglesia de Toledo. Ms. R.10, Biblioteca dela Escuela Técnica Superior de Arquitectura, Madrid.

Zessin, J., W. Lau, and J. Ochsendorf. 2010. Equilibrium of cracked masonry domes. *ICE Journal of Engineering and Computational Mechanics* 163 (3): 135–146.